Hindawi Publishing Corporation
International Journal of Spectroscopy
Volume 2014, Article ID 289638, 9 pages
http://dx.doi.org/10.1155/2014/289638

Research Article

The Application of Simple and Easy to Implement Decoupling Pulse Scheme Combinations to Effect Decoupling of Large J Values with Reduced Artifacts

Karel D. Klika

Molecular Structure Analysis, German Cancer Research Center (DKFZ), Im Neuenheimer Feld 280, 69009 Heidelberg, Germany

Correspondence should be addressed to Karel D. Klika; klikakd@yahoo.co.uk

Received 15 January 2014; Revised 29 March 2014; Accepted 31 March 2014; Published 29 April 2014

Academic Editor: Karol Jackowski

Of the various problems in decoupling one nucleus type from another using standard decoupling pulse schemes for broadband decoupling, a particular challenge is to effect full, artifact-free decoupling when the size of the coupling constant is very large. Herein it is demonstrated that ^{1}H decoupling of the ^{31}P NMR spectrum of diethyl phosphonate $\{HP(=O)(OCH_2CH_3)_2\}$ can be accomplished with reduced artifacts despite the large $^{1}J_{H,P}$ value of 693 Hz by using a combination of decoupling pulse schemes involving continuous-wave (CW) irradiation and either adiabatic-pulse decoupling (APD), MPF decoupling, or traditional composite-pulse decoupling (CPD) schemes such as WALTZ or GARP. The considered strategy is simple, efficient, and easy to implement on most instruments. The best result was attained for a combination of CW and CPD using GARP with a standard pulse width of 60 μs. Altogether, the advantages of the methodology include low power requirements, complete decoupling, tolerance of a range of large J values, large bandwidth for normal-sized J values, and the suppression of sidebands.

1. Introduction

Considerable strides have been made in terms of pulse development for NMR over and above the standard hard rectangular pulses and these advances include the development of composite pulses and shaped pulses as well as adiabatic pulses [1–8]. These advances are especially pertinent for decoupling applications with adiabatic pulses such as the CHIRP pulses [7–11] being at the very forefront of many of the improvements in broadband decoupling pulse schemes which is a critical aspect for heteronuclear experiments involving ^{13}C or ^{15}N nuclei, amongst others, due to the wide spectral ranges of these nuclei. Indeed, there are many challenges in decoupling one nucleus type from another [5, 8, 12–19]. These challenges, in addition to attaining effective decoupling over the full spectral range of the irradiated nucleus, include attaining complete or full decoupling, limiting artifacts such as sidebands, limiting the induced heating of the sample, and limiting the load on the decoupling coil, as well as tolerance of spectrometer performance in terms of pulse width (length) error, B_2 inhomogeneity, and phase-shift error. Consequently, a myriad of decoupling pulse schemes have been designed utilizing shaped pulses and other refinements to meet these challenges and overcome the shortcomings of older decoupling methods.

Though many decoupling pulse schemes in current use such as the conventional composite-pulse decoupling (CPD) methods WALTZ [14, 15] and GARP [16] still utilize hard rectangular pulses, they are nevertheless highly effective if used within their prescribed capabilities and specifications and are duly appropriately parameterized [8]. Despite the considerable advantages of the more advanced decoupling pulse schemes utilizing shaped pulses and other refinements over conventional CPD, for example, MPF decoupling methods [17–19] and adiabatic-pulse decoupling (APD) methods [2–7, 9, 11, 12, 20], they are not without their problems either. For example, the presence of sidebands under APD can readily exceed that of CPD methods [5, 7, 9–12, 17, 20]. Notwithstanding, there have been efforts to deal with these artifacts in APD [7, 9, 11, 12, 20] given the clear advantages of using adiabatic pulses in decoupling pulse schemes. Notable means of suppressing sidebands in APD

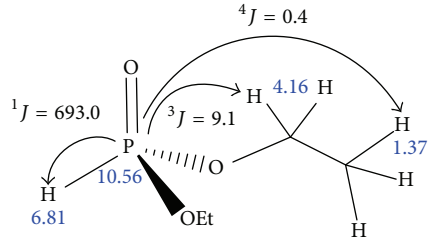

FIGURE 1: The structure of diethyl phosphonate with the ^{1}H–^{31}P couplings given in Hertz and the ^{1}H and ^{31}P δ values (in blue italic script) given in ppm.

include apodization of the adiabatic pulses [9, 11], use of fractional initial decoupling periods [12], application of the SEAD pulse sequence [20], and matching the sweep rate and direction to the coupling [20]. The need to minimize or eliminate altogether artifacts such as sidebands is not just a question of aesthetics; the presence of sidebands can reduce sensitivity as well as interfere with the analysis of multiple components through overlap; this is especially of concern for minor components whose intensity might be comparable to, or even be swamped by, sidebands emanating from the strong signal(s).

A particular interesting and challenging problem, though not necessarily often encountered when dealing primarily with ^{1}H, ^{13}C, ^{15}N, ^{31}P, or ^{19}F nuclei where for the most part coupling constants tend to be manageable, for example, $^{n}J_{H,H}$, $^{1}J_{H,C}$, $^{1}J_{H,N}$, $^{n}J_{H,P}$, $^{n}J_{H,F}$, $^{1}J_{F,C}$, and so forth, is that of attaining complete and artifact-free decoupling when the size of the coupling constant is very large since the decoupling proficiency of decoupling pulse schemes has a degree of J dependency [8, 9, 11, 15, 17, 19]. An example of large J is exhibited by diethyl phosphonate $\{HP(=O)(OCH_2CH_3)_2\}$ where the $^{1}J_{H,P}$ coupling is a rather sizeable 693 Hz (Figure 1).

The large value of $^{1}J_{H,P}$ is problematic for the hard rectangular pulses used in CPD methods such as WALTZ if the frequency of ^{1}H irradiation (ν_{irr}) is not on resonance in the case of observing the ^{13}P NMR spectrum while irradiating ^{1}H. That is, ν_{irr} should be placed in the middle of the proton doublet for the hydrogen atom directly bound to the phosphorous atom in this instance for diethyl phosphonate. The essence of the problem arises from the differential off-resonance effects for the two lines of the doublet due to the disparity in their dispositions in terms of Hertz with respect to ν_{irr} when ν_{irr} is off-resonance in terms of the generation of sidebands noting that the bandwidth remains essentially unaffected. APD does not circumvent this problem as there is a time lag for the swept pulse to traverse between the lines of the doublet. To counter the detrimental effects of the size of a large J value, recommendations include using shorter decoupling pulse widths (and thus necessarily higher power). For adiabatic pulses, a pulse width much shorter than $1/J$ is suggested [11] while, for hard pulses, having $\gamma B_1/20\pi \geq J$ is recommended [17]. For a J value of 693 Hz, this translates into 1.44 ms and 46 μs, respectively. While CW decoupling can be very effective in dealing with a large J, it is not fully suitable in the present case for the ^{31}P NMR spectrum since the coupling hydrogens are located across a range of δs (see Figure 1) and thus complete decoupling is not attainable. Also, a high amount of power is required placing considerable load on the coil. Nonetheless, the result can be unmatched in terms of the lack of artifact generation.

Herein is demonstrated methodology to deal with the problem of decoupling a large J value as applied to diethyl phosphonate in ^{31}P NMR spectra by combining CW irradiation with either APD, MPF decoupling, or traditional CPD schemes such as WALTZ or GARP to attain full decoupling with reduced artifacts. The considered strategy is simple, efficient, and easy to implement on most instruments.

2. Experimental

NMR spectra were acquired using a Bruker Avance III NMR spectrometer equipped with three RF channels and a 5 mm, normal-configuration, dual-coil probe with z-axis gradient capability at a field strength of 9.4 T operating at 400.1, 162.0, and 100.6 MHz for ^{1}H, ^{31}P, and ^{13}C nuclei, respectively, at 303 K with samples contained in $CDCl_3$. ^{1}H, ^{13}C, and ^{31}P 90° observation pulses were calibrated in the usual manner on the 360°-null point on samples of 1% TMS, 50% CH_2Cl_2, and ~5% diethyl phosphonate, respectively. Pulse widths and power levels for standard CPD methods were calibrated by first searching for suitable power levels at a desired decoupling pulse width with observation of ^{13}C or ^{31}P nuclei and decoupling by the CPD in question followed by refinement of the pulse width at a set power level selected from the aforementioned measurements. MPF and adiabatic pulses were used with set pulse widths with the power level similarly calibrated as just described for the CPD methods. Pulse widths (PW) and power levels (PL) are provided in the figure captions for each spectrum (vide infra). The performance of the finally selected pulse widths and power levels of all decoupling methods were confirmed by measurement of their effective decoupling bandwidths (DBs). DBs were assessed in the usual manner by acquiring a series of spectra with increasing amounts of offsets for ν_{irr}. DB limits were defined by when the intensity dropped to 75% of the maximum value. Sideband decoupling bandwidths (SDBs) limits were defined by when the intensity of the sidebands reached 1.5% of the aximum value. If the SDB is the same as or exceeds the DB, then its actual value was deemed as irrelevant since the limit value for useful decoupling is then set by the DB. DBs and SDBs are provided in the figure captions for each spectrum (vide infra). Samples utilized consisted of 50% CH_2Cl_2 and ~5% diethyl phosphonate for decoupling purposes. Decoupling pulse sequences WALTZ65, GARP4, and MPF7 were standard sequences and were used as provided in the vendor-supplied NMR software (Topspin 2.1.6) while APD used a phase cycling combination of Pines [21] and Levitt (MLEV4 [22]): $\{(0, 150, 60, 150, 0)_2 \ (180, 330, 240, 330, 180)_2\}$. Adiabatic smoothed CHIRP pulses were specifically generated using the Shape Tool subroutine of Topspin; the preferred one of several tested was designed for 42 kHz DB with 20% smoothing and defined

by 2 k pts. Pulse programs for acquisition consisted of single-pulse acquisition with inverse-gated decoupling in addition to single-pulse acquisition for the determination of coupling constants. ^{1}H NMR spectra were acquired with flip angles of 30° and an acquisition time (Aq) of 2.05 s and 3 s for the postacquisition delay (PAD); ^{13}C NMR spectra were acquired with flip angles of 30° and an Aq of 2.83 s and 2 s for the PAD; and ^{31}P NMR spectra were acquired with flip angles of 50° and an Aq of 2.02 s and 3 s for the PAD. Spectra were processed with zero-filling (fourfold) and the application of 0, 1, or 2 Hz of line broadening for ^{1}H, ^{13}C, and ^{31}P NMR spectra, respectively; for spin analysis, Gaussian transformation was applied to resolve small couplings and/or small $\Delta\delta$ as required; for the evaluation of linewidths (width at half-height, $\nu_{1/2}$) in ^{31}P NMR spectra, 0 Hz of line broadening was applied. For ^{31}P NMR spectra displayed herein, 2 Hz of line broadening was applied unless indicated otherwise. NMR spectra were referenced relative to TMS incorporated as an internal standard for ^{1}H and ^{13}C nuclei (δ = 0 ppm for both nuclei) while ^{31}P NMR spectra were referenced externally to 90% H_3PO_4 in D_2O (δ = 0 ppm). General NMR experimental details have been described previously [23–26] for routine assignment and analysis of couplings using 2D NMR and selective decouplings with confirmation where required by acquisitions of ^{1}H, ^{31}P, and ^{13}C NMR spectra at 14.1 T. Samples were routinely spun at a rate of 20 Hz unless stated otherwise since differences were not observed between the sidebands of rotated and stationary samples. Minor artifacts denoted as spinning sidebands were identified as such by acquiring spectra without spinning. In this work, the best result was attained for a combination of CW and CPD using GARP with a standard pulse width of 60 μs. Calibration of the power level required can be accomplished in a simple and rapid manner by the usual means as described above.

Diethyl phosphonate NMR data ($CDCl_3$): δ_H: 6.813 (dsp, $^{1}J_{H,P}$ = 693.01 and $^{5}J_{H,H}$ = 0.31 Hz, PH), 4.1568, 4.1564, and 4.1550 (3 × dqt, $^{3}J_{H,P}$ = 9.16, 9.16, and 9.07, resp., and $^{3}J_{H,H}$ = 7.09, 7.09, and 7.05, resp., Hz, $^{2}J_{H,H}$ not discernible, CH_2), and 1.370 (tt, $^{3}J_{H,H}$ = 7.08 and $^{4}J_{H,P}$ = $^{5}J_{H,H}$ = 0.32 Hz, CH_3); δ_C: 61.86 (tdqtd, $^{1}J_{H,C}$ = 147.89, $^{2}J_{C,P}$ = 5.69, $^{2}J_{H,C}$ = 4.45, and $^{3}J_{H,C}$ = 1.26 Hz, CH_2) and 16.34 (qtdt, $^{1}J_{H,C}$ = 127.36, $^{3}J_{C,P}$ = 6.20, and $^{2}J_{H,C}$ = 2.60 Hz, CH_3); δ_P: 10.56 (dqnsp, $^{1}J_{H,P}$ = 693.02, $^{3}J_{H,P}$ = 9.10, and $^{4}J_{H,P}$ = 0.40 Hz). {Note: abbreviations refer to standard meanings and describe the signals under resolution enhancement. The ethyl groups were distinguishable only by the ^{1}H resonances of the methylene signals while the methylene hydrogens within each ethyl group were only just distinguishable for one pair.}

3. Results and Discussion

Irrespective of the mode of decoupling applied—WALTZ, GARP, MPF, or APD—sidebands are noticeably apparent. Examples are presented in Figures 2 and 3 for the ^{31}P NMR of diethyl phosphonate indicating the sideband problem and the relative signal intensities of the main signal, respectively,

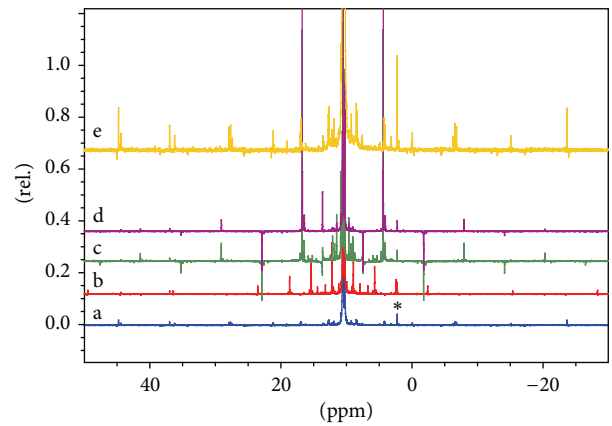

Figure 2: The ^{31}P NMR spectrum of $HP(=O)(OCH_2CH_3)_2$ indicates the resultant sidebands with decoupling of ^{1}H by (a) CPD decoupling using WALTZ (PW, 60 μs; PL, 10 dB; $\nu_{1/2}$, 1.33 Hz; DB, 10 kHz; SDB, 5 kHz); (b) CPD decoupling using GARP (PW, 60 μs; PL, 9.4 dB; $\nu_{1/2}$, 1.35 Hz; DB, 19 kHz; SDB, 7 kHz); (c) MPF decoupling (PW, 1 ms; PL, 11.3 dB; $\nu_{1/2}$, 1.32 Hz; DB, 28 kHz; SDB, 7 kHz); (d) APD using CHIRP (PW, 1 ms; PL, 5.8 dB; $\nu_{1/2}$, 1.47 Hz; DB, 44 kHz; SDB, 15 kHz); and (e) the same as (a) but with higher amplification to highlight the sidebands. The signal of a minor impurity (~3%) at 2.24 ppm is indicated with an asterisk. Note: all spectra within this figure, and similarly for spectra within the following figures, have been acquired with the same number of scans and receiver gain and processed in exactly the same way with identical line broadening and amplification unless explicitly stated otherwise. Legend: PW, pulse width (length); PL, power level; $\nu_{1/2}$, linewidth (width at half-height); DB, decoupling bandwidth; and SDB, sideband decoupling bandwidth.

under each decoupling method. While sidebands of random phase are able to be averaged out by the acquisition of multiple scans [15] (confirmed in this work, data not shown), sidebands of coherent phase on the other hand can potentially be removed by means of phase cycling [15] if they are incoherent with respect to the signal itself. Of note, the sidebands in all cases apart from the spectrum acquired under WALTZ decoupling conditions completely override the signal of a minor impurity (~3%) at 2.24 ppm, though even in the case of WALTZ decoupling the identity of real signals is hard to fathom and the integration of minor signals can be severely compromised in any case. The relative intensities of the main signal do vary significantly according to the decoupling method in use with CPD decoupling using WALTZ giving the optimum sensitivity amongst these four acquisitions.

One approach to suppressing sidebands is to make the B_2 RF amplitude sufficiently large [15, 19], though this then introduces problems with power dissipation leading to induced heating of the sample as well as placing high loads on the decoupling coil. Thus, increasing the B_2 RF amplitude to counter larger J values has its limits but can be useful and this is demonstrated for WALTZ and GARP CPD decoupling in Figures 4 and 5 showing a comparison of each decoupling method at both low and high power wherein the PW was decreased from 60 μs to 45 μs. In Figure 4, it can be seen that

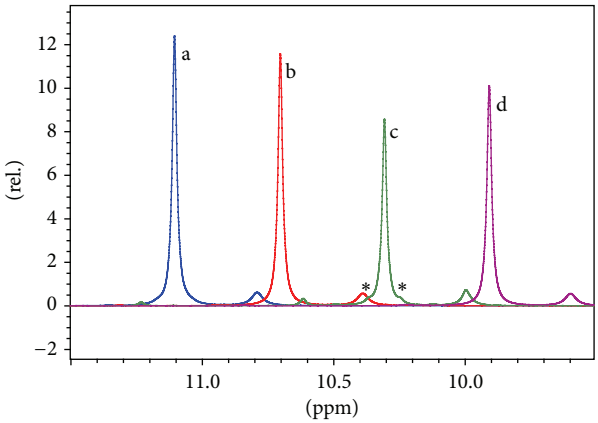

Figure 3: The ^{31}P NMR spectrum of HP(=O)$(OCH_2CH_3)_2$ indicates the relative sensitivities of the resultant signal with decoupling of ^{1}H by (a) CPD decoupling using WALTZ (PW, 60 μs; PL, 10 dB; $\nu_{1/2}$, 1.33 Hz; DB, 10 kHz; SDB, 5 kHz); (b) CPD decoupling using GARP (PW, 60 μs; PL, 9.4 dB; $\nu_{1/2}$, 1.35 Hz; DB, 19 kHz; SDB, 7 kHz); (c) MPF decoupling (PW, 1 ms; PL, 11.3 dB; $\nu_{1/2}$, 1.32 Hz; DB, 28 kHz; SDB, 7 kHz); and (d) APD using CHIRP (PW, 1 ms; PL, 5.8 dB; $\nu_{1/2}$, 1.47 Hz; DB, 44 kHz; SDB, 15 kHz). Note: the usual conditions for ^{1}H decoupling of ^{13}C spectra are represented by those given for (a) using WALTZ decoupling. Note that the signals present near the base of the signal for (c) marked with asterisks are not residual ^{1}H couplings but are the ^{13}C satellites ($2 \times {}^2J_{C,P}$ = 5.69 Hz and ($2 \times {}^3J_{C,P}$ = 6.20 Hz)—in this instance they are evident due to the particularly narrow base of the signal under MPF decoupling conditions but are readily discernible for other decoupling methods if 0 Hz line broadening is applied. A minor impurity signal (all cases) and sidebands (especially for MPF decoupling) are also evident.

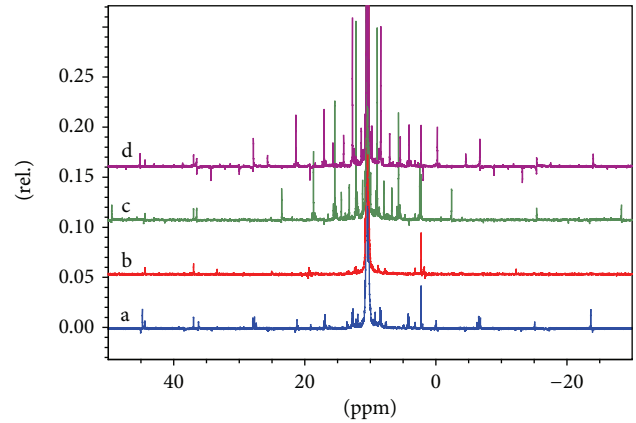

Figure 4: The ^{31}P NMR spectrum of HP(=O)$(OCH_2CH_3)_2$ indicates the resultant sidebands with decoupling of ^{1}H by (a) CPD decoupling using WALTZ (PW, 60 μs; PL, 10 dB; $\nu_{1/2}$, 1.33 Hz; DB, 10 kHz; SDB, 5 kHz); (b) CPD decoupling using WALTZ (PW, 45 μs; PL, 6 dB; $\nu_{1/2}$, 1.45 Hz; DB, 15 kHz; SDB, 3 kHz); (c) CPD decoupling using GARP (PW, 60 μs; PL, 9.4 dB; $\nu_{1/2}$, 1.35 Hz; DB, 19 kHz; SDB, 7 kHz); and (d) CPD decoupling using GARP (PW, 45 μs; PL, 7.4 dB; $\nu_{1/2}$, 1.43 Hz; DB, 26 kHz; SDB, 9 kHz).

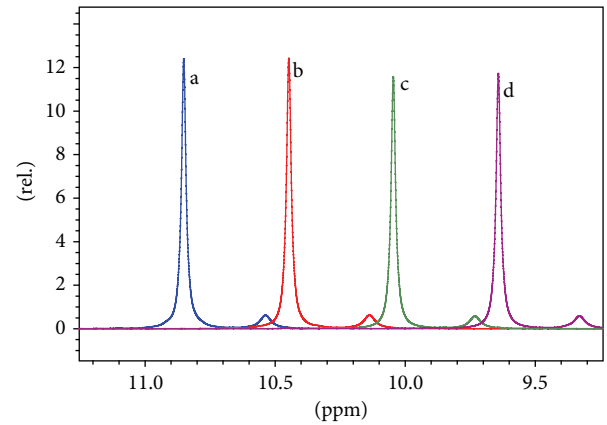

Figure 5: The ^{31}P NMR spectrum of HP(=O)$(OCH_2CH_3)_2$ indicates the relative sensitivities of the resultant signal with decoupling of ^{1}H by (a) CPD decoupling using WALTZ (PW, 60 μs; PL, 10 dB; $\nu_{1/2}$, 1.33 Hz; DB, 10 kHz; SDB, 5 kHz); (b) CPD decoupling using WALTZ (PW, 45 μs; PL, 6 dB; $\nu_{1/2}$, 1.45 Hz; DB, 15 kHz; SDB, 3 kHz); (c) CPD decoupling using GARP (PW, 60 μs; PL, 9.4 dB; $\nu_{1/2}$, 1.35 Hz; DB, 19 kHz; SDB, 7 kHz); and (d) CPD decoupling using GARP (PW, 45 μs; PL, 7.4 dB; $\nu_{1/2}$, 1.43 Hz; DB, 26 kHz; SDB, 9 kHz).

the sidebands are considerably reduced upon increased B_2 RF amplitude, especially for WALTZ decoupling where they are close to being eliminated altogether though it comes at the cost of some disruption to the base of the main signal. For GARP decoupling, though the largest sidebands are reduced in intensity, overall there seem to be more sidebands present. As well, the decoupling bandwidths (DBs) are also enlarged in both cases though in fact a smaller sideband decoupling bandwidth (SDB, vide infra) results for WALTZ decoupling. It is also interesting to note that, for both WALTZ and GARP decoupling, increasing the B_2 RF amplitude leads to slightly increased sensitivity despite increased $\nu_{1/2}$s (Figure 5).

For proficient decoupling, both lines of a doublet need to be equally perturbed [15]; for CPD, this is a problem when J is large due to differential off-resonance effects unless the frequency of irradiation (ν_{irr}) is placed on resonance of the coupled spin partner wherein both lines suffer equal off-resonance effects by virtue of being equidistant from ν_{irr}. For APD, problems persist as there is a time differential for the swept pulse to traverse between the lines of the doublet. Thus, with large J values, the position of ν_{irr} in standard decoupling pulse sequences can have a determinate effect on decoupling effectiveness with even small alterations to its value causing a noticeable change in the decoupling proficiency. This is especially so when using "standard" decoupling conditions such as CPD methods (e.g., those which are applied to, and appropriately suitable for, normal carbon acquisition) whereby there are differential off-resonance effects for the various lines of the multiplet arising from their large separation in Hertz. In other words, though large J values do not effect a reduction in the DBs per se {the same bandwidth of 10 kHz was obtained for observation of ^{13}C ($^1J_{H,C}$ = 178 Hz in CH_2Cl_2) as for observation of ^{31}P ($^1J_{H,P}$ = 693 Hz in diethyl phosphonate) using WALTZ decoupling, for example, with the standard conditions determined on a sample of CH_2Cl_2}, ν_{irr} does, however, influence the extent to which sidebands are generated in the case of large J. Thus there

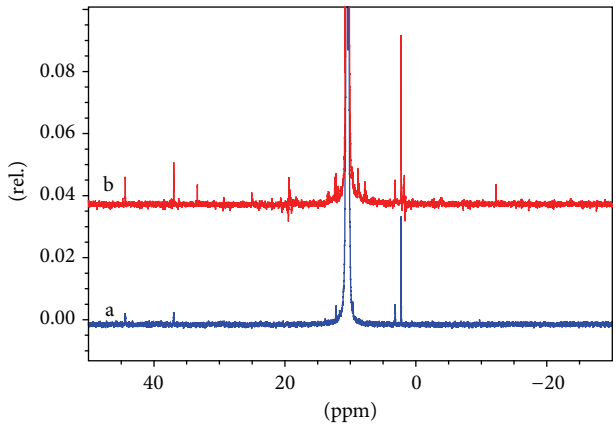

Figure 6: The ^{31}P NMR spectrum of HP(=O)$(OCH_2CH_3)_2$ indicates the resultant sidebands with decoupling of ^{1}H by (a) CW decoupling (PL, 5 dB; $\nu_{1/2}$, 3.85 Hz; DB, ~45 Hz; SDB, irrelevant) and (b) CPD decoupling using WALTZ (PW, 45 μs; PL, 6 dB; $\nu_{1/2}$, 1.45 Hz; DB, 15 kHz; SDB, 3 kHz).

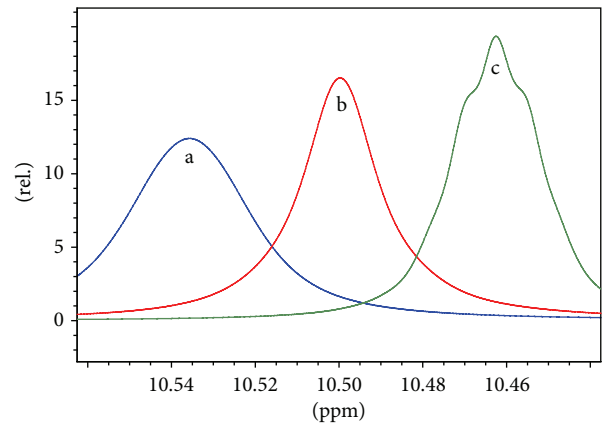

Figure 7: The ^{31}P NMR spectrum of HP(=O)$(OCH_2CH_3)_2$ indicates the relative sensitivities of the resultant signal with decoupling of ^{1}H by (a) CW decoupling (PL, 5 dB; $\nu_{1/2}$, 3.85 Hz; DB, ~45 Hz; SDB, irrelevant) and (b) CPD decoupling using WALTZ (PW, 45 μs; PL, 6 dB; $\nu_{1/2}$, 1.45 Hz; DB, 15 kHz; SDB, 3 kHz) and (c) the same as (a) except with the application of 0 Hz line broadening to reveal the residual coupling to the methylene protons.

is, in addition to the DB, the concept of the SDB, that is, the frequency range over which the size and extent of the sidebands generated by the decoupling method are tolerable (in this case, defined by convenience as 1.5% of the main signal ≈50% of a minor signal). This frequency range can be considerably narrower than the DB and varies inconsistently with the size of the DB, while it is heavily dependent on the decoupling method in addition to other factors; in particular, the SDB is J dependent.

One method that does not engender sidebands is CW decoupling, though it comes with a requirement for high power and the need to effectively set ν_{irr} on resonance; hence it is limited to possessing only a very restricted DB. Thus in the case of multiple species and/or multiple spin coupling partners, not all couplings can be fully eliminated. Since ν_{irr} needs to be set basically on resonance, this may be problematic in ascertaining in the case of dilute or complex samples though this is not generally a difficult problem. Obviously the presence of multiple species cannot be handled effectively unless they are all essentially very similar, and finally, also readily evident, wide δ ranges cannot be handled either in the case of multiple spin partners with diethyl phosphonate being a case in point here. The advantages and shortcomings of CW decoupling are readily evident in Figures 6 and 7. The improvement in the sidebands is remarkable, and furthermore, the real signals are clearly identifiable, though those with large offsets for ν_{irr} can lose considerably in intensity. For example, even the signal of the minor impurity at 2.24 ppm is clearly of lower intensity (~40%) in the CW decoupled spectrum in comparison to the spectrum acquired with WALTZ decoupling at high power, even more so than for the main signal (~25%), while the signal at 36.96 ppm is lower by ~75%. This problem for CW decoupling, aside from large power demands, is further illustrated in Figure 7 wherein with the application of 0 Hz line broadening, the coupling of the main signal to the methylene protons that is not fully eliminated can clearly be seen. Indeed, with the large size of the $^1J_{H,P}$ coupling in diethyl phosphonate, the effective bandwidth is only ~45 Hz; in other words, ν_{irr} needs to be essentially on resonance, or at least very close to it, and thus the δ_H needs to be accurately known for CW to be effective in cases of large J. Of note though, not only the decoupling sidebands but also the spinning sidebands are reduced (but not fully eliminated) with CW decoupling (data not shown) and the base of the peak is much improved in comparison to the WALTZ decoupling with high power. These attributes, and the fact that CW decoupling is tolerant of the actual size of J when ν_{irr} is on resonance, are the great advantages of CW decoupling. Indeed, disregarding the incomplete decoupling arising from the methylene protons resonating distal to ν_{irr}, the spectrum obtained using CW decoupling is virtually pristine.

The strategy considered here to overcome the problem of a large J value, which is a particular source of the sidebands, was to combine CW decoupling with other decoupling pulse sequences by applying both simultaneously. Thereby the desirable features of CW decoupling are exploited together with the incorporation of the broad bandwidth of the other decoupling techniques. CW decoupling facilitates the improved decoupling efficiency of a decoupling pulse sequence even if not fully proficient at the power level used, or if not perfectly on resonance, as it results in an effectively reduced coupling constant. In this methodology, the ^{1}H frequencies, one for the CW decoupling and the other for the broad bandwidth decoupling pulse sequences, were generated in separate oscillators but routed to the one amplifier before transfer to the high-frequency coil of the probe. By this manner, there is a superposition of decoupling signals applied simultaneously to the sample.

While only a dual-coil at the minimum is required for this technique, and only two amplifiers (with inclusion of the amplifier needed to generate pulses for the observed nucleus),

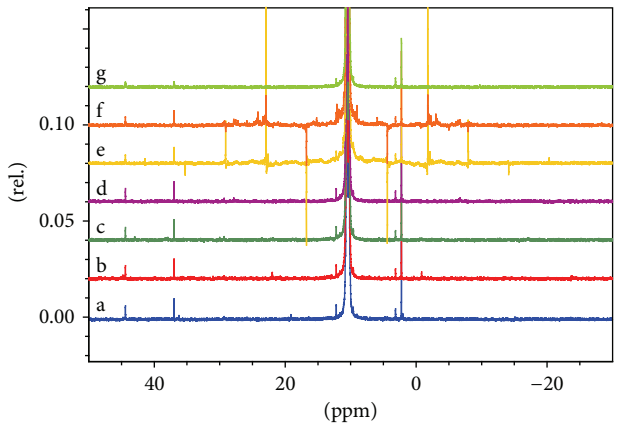

Figure 8: The ^{31}P NMR spectrum of HP(=O)$(OCH_2CH_3)_2$ indicates the resultant sidebands with decoupling of ^{1}H by (a) CPD decoupling using WALTZ and CW (PW, 60 μs; PL, 12.4 dB; $\nu_{1/2}$, 1.35 Hz; DB, 400 Hz; SDB, 150 Hz); (b) CPD decoupling using WALTZ and CW (PW, 45 μs; PL, 11.4 dB; $\nu_{1/2}$, 1.37 Hz; DB, 2 kHz; SDB, 1 kHz); (c) CPD decoupling using GARP and CW (PW, 60 μs; PL, 10.6 dB; $\nu_{1/2}$, 1.41 Hz; DB, 1 kHz; SDB, 400 Hz); (d) CPD decoupling using GARP and CW (PW, 45 μs; PL, 10.9 dB; $\nu_{1/2}$, 1.55 Hz; DB, 700 Hz; SDB, irrelevant); (e) MPF and CW decoupling (PW, 1 ms; PL, 15.8 dB; $\nu_{1/2}$, 1.50 Hz; DB, 120 Hz; SDB, irrelevant); (f) APD decoupling using CHIRP and CW (PW, 1 ms; PL, 15.2 dB; $\nu_{1/2}$, 1.48 Hz; DB, 250 Hz; SDB, irrelevant); and (g) CW decoupling (PL, 5 dB; $\nu_{1/2}$, 3.85 Hz; DB, ~45 Hz; SDB, irrelevant).

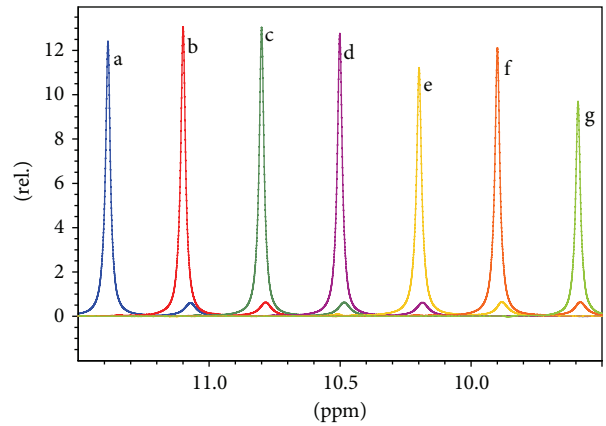

Figure 9: The ^{31}P NMR spectrum of HP(=O)$(OCH_2CH_3)_2$ indicates the relative sensitivities of the resultant signal with decoupling of ^{1}H by (a) CPD decoupling using WALTZ and CW (PW, 60 μs; PL, 12.4 dB; $\nu_{1/2}$, 1.35 Hz; DB, 400 Hz; SDB, 150 Hz); (b) CPD decoupling using WALTZ and CW (PW, 45 μs; PL, 11.4 dB; $\nu_{1/2}$, 1.37 Hz; DB, 2 kHz; SDB, 1 kHz); (c) CPD decoupling using GARP and CW (PW, 60 μs; PL, 10.6 dB; $\nu_{1/2}$, 1.41 Hz; DB, 1 kHz; SDB, 400 Hz); (d) CPD decoupling using GARP and CW (PW, 45 μs; PL, 10.9 dB; $\nu_{1/2}$, 1.55 Hz; DB, 700 Hz; SDB, irrelevant); (e) MPF and CW decoupling (PW, 1 ms; PL, 15.8 dB; $\nu_{1/2}$, 1.50 Hz; DB, 120 Hz; SDB, irrelevant); (f) APD decoupling using CHIRP and CW (PW, 1 ms; PL, 15.2 dB; $\nu_{1/2}$, 1.48 Hz; DB, 250 Hz; SDB, irrelevant); and (g) CW decoupling (PL, 5 dB; $\nu_{1/2}$, 3.85 Hz; DB, ~45 Hz; SDB, irrelevant).

three oscillators are necessary without the availability of an advanced and sophisticated pulse-shaping subroutine within the NMR software program. The use of a single amplifier restricts the applied power to be shared between the two decoupling methods and thus necessitates that they have equal demands for their power under the applied conditions. On more flexible and expanded NMR systems, separate amplifiers could have their signals routed to the one coil or separate coils altogether could be used to carry the decoupling frequencies.

One resulting necessary condition is that the ν_{irr} for both the CW and the broadband decoupling scheme need to be the same; this is a consequence of irregular convolution of the generated frequency pattern arising from the two irradiations yielding poor decoupling if the two ν_{irr}s are different. Thus the ν_{irr} for the broadband decoupling scheme is "bound" to the ν_{irr} for CW decoupling and as a consequence the ν_{irr} for the broadband decoupling scheme cannot be transposed over a reasonable range due to the limitations of the CW decoupling. This is not as restrictive as it may initially seem as the broadband capability of the broadband decoupling scheme for normal size coupling remains in place and the decoupling of multiple large Js differing in sizeable δ would not be effected by the frequency-restricted nature of CW decoupling in any case; that is, multiple large couplings cannot be fully decoupled if they differ by sizeable δ for the coupled spins concerned. However, the δ of the coupling protons for the large coupling must be known, or at least reasonably approximated, though this is usually quite easily done in any event by acquisition of, for example, HSQC spectra if not already evident by inspection. Since normal size couplings spanning large spectral ranges can still be eliminated by the broadband decoupling, in effect there are three DBs to consider, namely, the DB for large J values, the DB for normal J values, and the SDB.

In Figures 8 and 9 are presented the results of such a strategy for the combination of CW decoupling with various other decoupling pulse sequences. It can be seen that in all cases the sidebands are much reduced, almost to the point of matching that attained by CW decoupling for the application of CPD using either WALTZ or GARP using either standard PWs (60 μs) or the shorter PWs (45 μs) applied above. Interestingly, the spectra acquired with 60 μs for both WALTZ and GARP match, or are even better than, the spectra acquired with 60 μs in this combination mode in contrast to the previous comparison. Indeed, the best result is attained for CPD using GARP and the standard PW of 60 μs. Also, these four CPD spectra all have a base of the peak comparable to that acquired with CW decoupling. Also notable is the fact that the sensitivity is high due to the signal not being distributed to the sidebands. Of most note, the power levels in use are considerably lower than that required for CW decoupling and also for single decoupling mode. The tolerance of the set power level for these combined decoupling methods is very high; often a range spanning 1.6 dB yielded similar results to the optimized set value; in the case of GARP decoupling, this extended to 4 dB. The full decoupling attained is perhaps the most notable feature after the suppression of the sidebands, and this is in stark contrast to the CW decoupling. The tolerance for the large

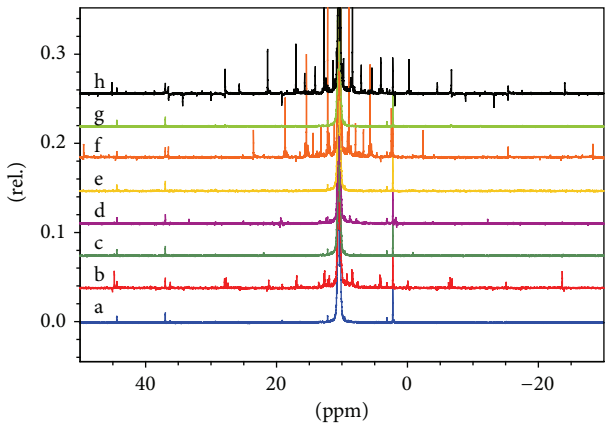

Figure 10: The ^{31}P NMR spectrum of HP(=O)$(OCH_2CH_3)_2$ indicates the resultant sidebands with decoupling of ^{1}H by (a) CPD decoupling using WALTZ and CW (PW, 60 μs; PL, 12.4 dB; $\nu_{1/2}$, 1.35 Hz; DB, 400 Hz; SDB, 150 Hz); (b) CPD decoupling using WALTZ (PW, 60 μs; PL, 10 dB; $\nu_{1/2}$, 1.33 Hz; DB, 10 kHz; SDB, 5 kHz); (c) CPD decoupling using WALTZ and CW (PW, 45 μs; PL, 11.4 dB; $\nu_{1/2}$, 1.37 Hz; DB, 2 kHz; SDB, 1 kHz); (d) CPD decoupling using WALTZ (PW, 45 μs; PL, 6 dB; $\nu_{1/2}$, 1.45 Hz; DB, 15 kHz; SDB, 3 kHz); (e) CPD decoupling using GARP and CW (PW, 60 μs; PL, 10.6 dB; $\nu_{1/2}$, 1.41 Hz; DB, 1 kHz; SDB, 400 Hz); (f) CPD decoupling using GARP (PW, 60 μs; PL, 9.4 dB; $\nu_{1/2}$, 1.35 Hz; DB, 19 kHz; SDB, 7 kHz); (g) CPD decoupling using GARP and CW (PW, 45 μs; PL, 10.9 dB; $\nu_{1/2}$, 1.55 Hz; DB, 700 Hz; SDB, irrelevant); and (h) CPD decoupling using GARP (PW, 45 μs; PL, 7.4 dB; $\nu_{1/2}$, 1.43 Hz; DB, 26 kHz; SDB, 9 kHz).

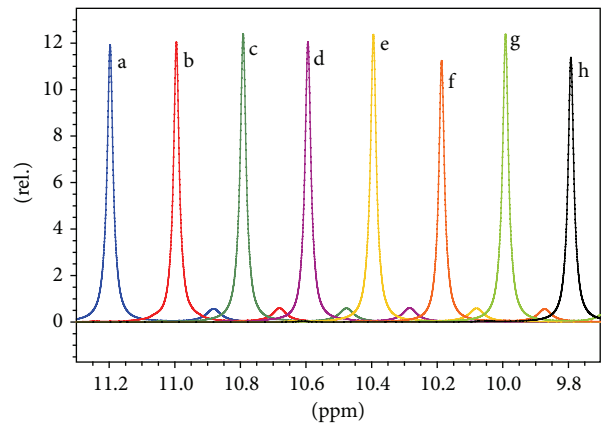

Figure 11: The ^{31}P NMR spectrum of HP(=O)$(OCH_2CH_3)_2$ indicates the relative sensitivities of the resultant signal with decoupling of ^{1}H by (a) CPD decoupling using WALTZ and CW (PW, 60 μs; PL, 12.4 dB; $\nu_{1/2}$, 1.35 Hz; DB, 400 Hz; SDB, 150 Hz); (b) CPD decoupling using WALTZ (PW, 60 μs; PL, 10 dB; $\nu_{1/2}$, 1.33 Hz; DB, 10 kHz; SDB, 5 kHz); (c) CPD decoupling using WALTZ and CW (PW, 45 μs; PL, 11.4 dB; $\nu_{1/2}$, 1.37 Hz; DB, 2 kHz; SDB, 1 kHz); (d) CPD decoupling using WALTZ (PW, 45 μs; PL, 6 dB; $\nu_{1/2}$, 1.45 Hz; DB, 15 kHz; SDB, 3 kHz); (e) CPD decoupling using GARP and CW (PW, 60 μs; PL, 10.6 dB; $\nu_{1/2}$, 1.41 Hz; DB, 1 kHz; SDB, 400 Hz); (f) CPD decoupling using GARP (PW, 60 μs; PL, 9.4 dB; $\nu_{1/2}$, 1.35 Hz; DB, 19 kHz; SDB, 7 kHz); (g) CPD decoupling using GARP and CW (PW, 45 μs; PL, 10.9 dB; $\nu_{1/2}$, 1.55 Hz; DB, 700 Hz; SDB, irrelevant); and (h) CPD decoupling using GARP (PW, 45 μs; PL, 7.4 dB; $\nu_{1/2}$, 1.43 Hz; DB, 26 kHz; SDB, 9 kHz).

J values can be expected to be high (based on the tolerance of CW decoupling to such), though this is difficult to test in practicality without numerous appropriate examples on hand, and also for the bandwidth of normal-sized J values (based on the tolerance of broadband decoupling pulse schemes to such), although this too is difficult to test in practicality without numerous appropriate examples on hand since the ν_{irr} is restrained by the CW decoupling in use. Thus while the bandwidth for large J is measurably small, the bandwidth for normal J to all intents and purposes should be sizeable and is definitely sufficient in this instance. Needless to say, the SDB is also similarly constrained as for the bandwidth for large J.

To illustrate better the gains acquired, in Figures 10 and 11 are presented the spectra acquired using CPD with either WALTZ or GARP decoupling at both standard and short PW conditions for both single decoupling mode and in combination with CW. In all four cases, the results can be considered spectacular. Except for WALTZ decoupling with spectra acquired with 60 μs PW where the sensitivity is essentially unchanged upon using the combination mode, there are slight increases in sensitivity for the other three cases in comparison of the single decoupling mode versus the same decoupling in combination with CW.

For MPF decoupling and ADP, although the improvements when applying the CW combination mode in comparison to the single decoupling mode are still considerable as illustrated in Figure 12, they do not quite match the performance of the CPD methods. For MPF, the sidebands still dominate the signal of the minor impurity at 2.24 ppm while for ADP the sidebands are much less than the 3% intensity of that signal. Nevertheless, they may offer a larger DB for normal-sized couplings in comparison to the CPD methods, and this could be of value for nuclei spanning wide δ ranges in comparison to ^{1}H. Without a suitable selection of test samples on hand, this cannot be tested though. In both cases, however, there is a sensitivity gain as illustrated in Figure 13.

Thus, the results clearly indicate that the decoupling of a large J value can be proficiently accomplished whereby sidebands are much reduced; the signal is fully decoupled and has attained near minimum $\nu_{1/2}$ close to the intrinsic $\nu_{1/2}$ and thus the ultimate sensitivity permissible. Moreover, the methodology is likely to retain significant DB from the broadband decoupling pulse sequences and be effectively independent of the value of J in that it does not require substantial amendment of the decoupling parameters depending on its particular value, for example, by adjusting accordingly the decoupling pulse width [11, 17], sweep rate and direction of sweep [20], and so forth, since the major decoupling can be effected by the CW decoupling. Certainly the presence of a range of J values can easily be accommodated as well as the presence of multiple coupling partners. The only shortcoming would be the presence of multiple observed species with very different δs, though this could potentially be handled by multiple irradiation points. In this case here, the sidebands

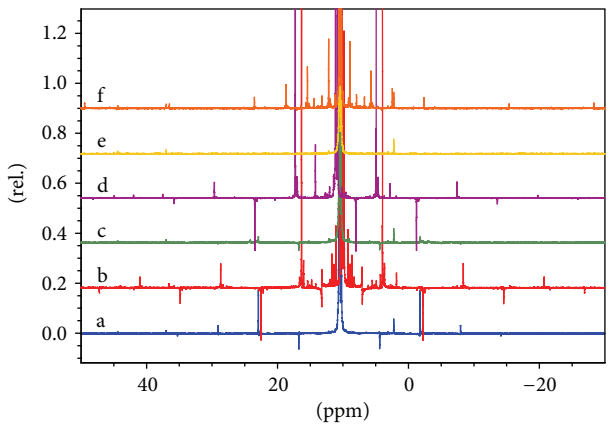

Figure 12: The ^{31}P NMR spectrum of HP(=O)$(OCH_2CH_3)_2$ indicates the resultant sidebands with decoupling of ^{1}H by (a) MPF and CW decoupling (PW, 1 ms; PL, 15.8 dB; $\nu_{1/2}$, 1.50 Hz; DB, 120 Hz; SDB, irrelevant); (b) MPF decoupling (PW, 1 ms; PL, 11.3 dB; $\nu_{1/2}$, 1.32 Hz; DB, 28 kHz; SDB, 7 kHz); (c) APD decoupling using CHIRP and CW (PW, 1 ms; PL, 15.2 dB; $\nu_{1/2}$, 1.48 Hz; DB, 250 Hz; SDB, irrelevant); (d) APD using CHIRP (PW, 1 ms; PL, 5.8 dB; $\nu_{1/2}$, 1.47 Hz; DB, 44 kHz; SDB, 15 kHz); (e) CPD decoupling using GARP and CW (PW, 60 μs; PL, 10.6 dB; $\nu_{1/2}$, 1.41 Hz; DB, 1 kHz; SDB, 400 Hz); and (f) CPD decoupling using GARP (PW, 60 μs; PL, 9.4 dB; $\nu_{1/2}$, 1.35 Hz; DB, 19 kHz; SDB, 7 kHz). Note: spectra (b) and (d) have been shifted in frequency slightly for ease of comparison.

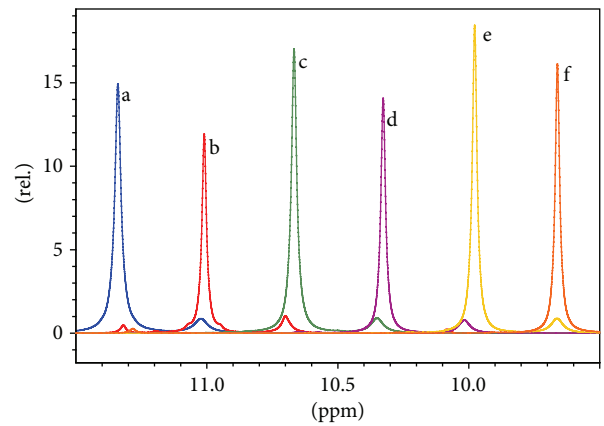

Figure 13: The ^{31}P NMR spectrum of HP(=O)$(OCH_2CH_3)_2$ indicates the relative sensitivities of the resultant signal with decoupling of ^{1}H by (a) MPF and CW decoupling (PW, 1 ms; PL, 15.8 dB; $\nu_{1/2}$, 1.50 Hz; DB, 120 Hz; SDB, irrelevant); (b) MPF decoupling (PW, 1 ms; PL, 11.3 dB; $\nu_{1/2}$, 1.32 Hz; DB, 28 kHz; SDB, 7 kHz); (c) APD decoupling using CHIRP and CW (PW, 1 ms; PL, 15.2 dB; $\nu_{1/2}$, 1.48 Hz; DB, 250 Hz; SDB, irrelevant); (d) APD using CHIRP (PW, 1 ms; PL, 5.8 dB; $\nu_{1/2}$, 1.47 Hz; DB, 44 kHz; SDB, 15 kHz); (e) CPD decoupling using GARP and CW (PW, 60 μs; PL, 10.6 dB; $\nu_{1/2}$, 1.41 Hz; DB, 1 kHz; SDB, 400 Hz); and (f) CPD decoupling using GARP (PW, 60 μs; PL, 9.4 dB; $\nu_{1/2}$, 1.35 Hz; DB, 19 kHz; SDB, 7 kHz).

of the large signal are problematic in assessing the veracity of the minor signals under normal conditions while clearly the sidebands of minor signals are inconsequential as might normally be the case for a single signal. Thus, it is fully evident that the signals of minor components, such as those at 2.24 and 36.96 ppm, are readily identifiable as real signals and are not compromised by the sidebands of the prominent signal and, furthermore, their intensities are amenable to correct evaluation. This gain is a considerable benefit for the analysis of such samples.

4. Conclusions

Herein it has been demonstrated that ^{1}H decoupling of the ^{31}P NMR spectrum of diethyl phosphonate {HP(=O)$(OCH_2CH_3)_2$} can be accomplished with reduced artifacts despite the large $^1J_{H,P}$ value of 693 Hz by using a combination of decoupling pulse schemes involving CW irradiation and either APD, MPF, or traditional CPD schemes such as WALTZ or GARP. The developed strategy is simple, efficient, and easy to implement on most instruments. Attaining full, artifact-free decoupling is not just a question of aesthetics as there are practical applications: in cases where sensitivity is important since sensitivity is lost when the usual decoupling pulse sequences are applied in cases of large J either due to the decoupling being incomplete or via the introduction artifact sidebands; when the resolution of signals is of importance; and finally, when small signals are of interest in the presence of large signals as the evaluation of the signals from the minor components is compromised by the sidebands arising from the signals of the large components. The best result was attained for a combination of CW and CPD using GARP with a standard pulse width of 60 μs. Altogether, the advantages of the methodology include low power requirements, complete decoupling, tolerance of a range of large J values, large bandwidth for normal-sized J values, and the suppression of sidebands.

Conflict of Interests

The author declares that there is no conflict of interests regarding the publication of this paper.

References

[1] T. L. Hwang, P. C. M. van Zijl, and M. Garwood, "Fast broadband inversion by adiabatic pulses," *Journal of Magnetic Resonance*, vol. 133, no. 1, pp. 200–203, 1998.

[2] M. Garwood and L. DelaBarre, "The return of the frequency sweep: designing adiabatic pulses for contemporary NMR," *Journal of Magnetic Resonance*, vol. 153, no. 2, pp. 155–177, 2001.

[3] A. Tannús and M. Garwood, "Adiabatic pulses," *NMR in Biomedicine*, vol. 10, no. 8, pp. 423–434, 1997.

[4] M. A. Smith, H. Hu, and A. J. Shaka, "Improved broadband inversion performance for NMR in liquids," *Journal of Magnetic Resonance*, vol. 151, no. 2, pp. 269–283, 2001.

[5] Ë. Kupče, R. Freeman, G. Wider, and K. Wüthrich, "Figure of merit and cycling sidebands in adiabatic decoupling," *Journal of Magnetic Resonance A*, vol. 120, no. 2, pp. 264–268, 1996.

[6] M. R. Bendall, "Heteronuclear J coupling precession during spin-lock and adiabatic pulses. use of adiabatic inversion pulses

in high-resolution NMR," *Journal of Magnetic Resonance A*, vol. 116, no. 1, pp. 46–58, 1995.

[7] T. Parella, NMR Guide 3.5, 1998–2003, http://triton.iqfr.csic.es/guide/eNMR/eNMRcomp/decoupling1.html.

[8] V. P. Ananikov, Ultrabroadband Heteronuclear Decoupling Methods, 1998, http://nmr.ioc.ac.ru/val/shapes/c-w/c-w.htm.

[9] R. Fu and G. Bodenhausen, "Evaluation of adiabatic frequency-modulated schemes for broadband decoupling in isotropic liquids," *Journal of Magnetic Resonance A*, vol. 119, no. 1, pp. 129–133, 1996.

[10] R. Fu and G. Bodenhausen, "Ultra-broadband decoupling," *Journal of Magnetic Resonance A*, vol. 117, no. 2, pp. 324–325, 1995.

[11] R. Fu and G. Bodenhausen, "Broadband decoupling in NMR with frequency-modulated "chirp" pulses," *Chemical Physics Letters*, vol. 245, no. 4-5, pp. 415–420, 1995.

[12] S. Zhang and D. G. Gorenstein, "Adiabatic Decoupling Sidebands," *Journal of Magnetic Resonance*, vol. 144, no. 2, pp. 316–321, 2000.

[13] S. Zhang and D. G. Gorenstein, "'Double-WURST' decoupling for ^{15}N- and ^{13}C-double-labeled proteins in a high magnetic field," *Journal of Magnetic Resonance A*, vol. 123, no. 2, pp. 181–187, 1996.

[14] A. J. Shaka, J. Keeler, T. Frenkiel, and R. Freeman, "An improved sequence for broadband decoupling: WALTZ-16," *Journal of Magnetic Resonance*, vol. 52, no. 2, pp. 335–338, 1983.

[15] A. J. Shaka, J. Keeler, and R. Freeman, "Evaluation of a new broadband decoupling sequence: WALTZ-16," *Journal of Magnetic Resonance*, vol. 53, no. 2, pp. 313–340, 1983.

[16] A. J. Shaka, P. B. Barker, and R. Freeman, "Computer-optimized decoupling scheme for wideband applications and low-level operation," *Journal of Magnetic Resonance*, vol. 64, no. 3, pp. 547–552, 1985.

[17] T. Fujiwara and K. Nagayama, "Composite inversion pulses with frequency switching and their application to broadband decoupling," *Journal of Magnetic Resonance*, vol. 77, no. 1, pp. 53–63, 1988.

[18] T. Fujiwara and K. Nagayama, "Optimized frequency/phase-modulated broadband inversion pulses," *Journal of Magnetic Resonance*, vol. 86, no. 3, pp. 584–592, 1990.

[19] T. Fujiwara, T. Anai, N. Kurihara, and K. Nagayama, "Frequency-switched composite pulses for decoupling carbon-13 spins over ultrabroad bandwidths," *Journal of Magnetic Resonance A*, vol. 104, no. 1, pp. 103–105, 1993.

[20] E. Kupče, "Effect of sweep direction on sidebands in adiabatic decoupling," *Journal of Magnetic Resonance*, vol. 129, no. 2, pp. 219–221, 1997.

[21] R. Tycko, A. Pines, and J. Guckenheimer, "Fixed point theory of iterative excitation schemes in NMR," *The Journal of Chemical Physics*, vol. 83, no. 6, pp. 2775–2802, 1985.

[22] M. H. Levitt and R. Freeman, "Composite pulse decoupling," *Journal of Magnetic Resonance*, vol. 43, no. 3, pp. 502–507, 1981.

[23] J. Mäki, P. Tähtinen, L. Kronberg, and K. D. Klika, "Restricted rotation/tautomeric equilibrium and determination of the site and extent of protonation in bi-imidazole nucleosides by multinuclear NMR and GIAO-DFT calculations," *Journal of Physical Organic Chemistry*, vol. 18, no. 3, pp. 240–249, 2005.

[24] P. Virta, A. Koch, M. U. Roslund et al., "Synthesis, characterisation and theoretical calculations of 2,6-diaminopurine etheno derivatives," *Organic and Biomolecular Chemistry*, vol. 3, no. 16, pp. 2924–2929, 2005.

[25] K. D. Klika, J. Bernát, J. Imrich, I. Chomča, R. Silanpää, and K. Pihlaja, "Unexpected formation of a spiro acridine and fused ring system from the reaction between an *N*-acridinylmethyl-substituted thiourea and bromoacetonitrile under basic conditions," *Journal of Organic Chemistry*, vol. 66, no. 12, pp. 4416–4418, 2001.

[26] E. Balentová, J. Imrich, J. Bernát et al., "Stereochemistry, tautomerism, and reactions of acridinyl thiosemicarbazides in the synthesis of 1,3-thiazolidines," *Journal of Heterocyclic Chemistry*, vol. 43, no. 3, pp. 645–656, 2006.